Desalination and Water Treatment
www.deswater.com
doi: 10.5004/dwt.2022.28086

249 (2022) 87–102
February

Adsorption technique for the removal of acetaminophen as adsorbate contaminant from water with metals and eggshell

Chima B. Njoku, Titus A.M. Msagati*

Institute for Nanotechnology and Water Sustainability, College of Science Engineering and Technology, The University of South Africa (Science Campus), 1709 Johannesburg, South Africa, Tel. +27 11 670 9482 (Office Line – Prof. Tam Msagati); emails: kutechi02@gmail.com (C.B. Njoku), msagatam@unisa.ac.za (T.A.M. Msagati)

Received 7 September 2021; Accepted 17 December 2021

ABSTRACT

Various classes of pharmaceutical drugs have been detected in different environmental compartments around the world. Research is being conducted to fully understand the environmental fate of pharmaceuticals, particularly non-steroidal anti-inflammatory drugs, discovered in South Africa in the near future. In this study, we synthesized iron/eggshell/bentonite (FEB) and eggshell/bentonite (EB) samples that extract acetaminophen from aqueous environmental samples. On the holes of the samples, acetaminophen was adsorbing by a Langmuir isotherm and by a pseudo-second-order model implying the formation of a monolayer through physical adsorption. Through the Langmuir model, we evaluated the nanocomposites' adsorption capacity on acetaminophen pharmaceutical for removal at 25°C using EB (16.55 mg g^{-1}) and FEB (46.34 mg g^{-1}). The FEB and EB were used as selective sorbents to extract acetaminophen from wastewater. UV/Vis chromatography was then performed to analyse the results. As a result of the analytical method, the detection limit was 0.109 and 0.133 mg mL^{-1} and recovery was 99.9%; concentrations of acetaminophen in wastewater samples ranged from 0.042 to 0.133 mg mL^{-1} for EB adsorbent and 0.023 to 0.109 mg mL^{-1} for FEB. Several studies have shown that wastewater in the labs can be treated effectively for the release of acetaminophen.

Keywords: Recovery; Acetaminophen; Wastewater; Physical adsorption; Eggshell; Bentonite; Nanocomposites

1. Introduction

There are many drugs in the world that are sold or called over the counter (OTC) drugs. Among them is acetaminophen (Acet), acetaminophen is used as a pain reliever by raising the threshold between no pain and severe pain, which means a person must feel significantly more pain to feel it. This drug reduces fever in part by acting on the heat-regulating center of the brain. Furthermore, acetaminophen is used to relieve mild to heavy pain from headaches, muscle aches, menstrual periods, colds and sore throats, toothaches, and backaches [1]. It is a water-soluble drug and can be eliminated as waste into sewage systems and can pollute groundwater and other bodies of water [2]. Conventional water treatment has been involved in remediating water bodies, but in the process these pharmaceuticals have not been removed easily, as they are regarded as "pseudo-persistent" [3,4].

In South Africa, we have been studying the removal of acetaminophen from our lakes, rivers, and dams [5,6]. However, this scientific process has caused these acetaminophens to be regarded as toxic to DNA, generates negative effects on natural materials, pathogenic microbes' resistors and endocrine disruptors [2]. The pharmaceuticals cause the problem of sickness as pollutants because of their extreme persistence and acute adverse effects, therefore

* Corresponding author.

1944-3994/1944-3986 © 2022 Desalination Publications. All rights reserved.

there is a need for remediation. Therefore, adsorption is a reliable method for removing pollutants, as it is an efficient method and it is simple to use [7,8]. It is also a reversible process that decreases with the rise in temperature. Among the other advantages adsorption process takes place relatively quickly, Equilibrium is reached in 1 h and the adsorbents are recyclable [9–12]. Adsorption is also the process by which it is proportional to the surface area, it could vary with the nature of the surface of the adsorbent and the substance deposited onto the surface of a solid (adsorbent or sorbent) [13]. Furthermore, when adsorptive surfaces are present, many chemical reactions are speeded up. This surface adsorption facilitates to mix adsorbates with substrates to give reaction products. The adsorption methods taking place encourage many essential chemical reactions and also produce changes in surface tension. Drugs which are adsorbed on the adsorbent surfaces put forth their effects from that location.

Adsorption of drug particles like acetaminophen particles on the surface has been extensively used in the pharmaceutical industry for several purposes, such as improving the content uniformity of low dose drugs, improving the dissolution rate for poorly water soluble drugs and enhancing some special formulation designs. Attaining good content uniformity is a common challenge when making solid dosage formulations. The most frequently used approaches is adsorbing small drug particles at the surface of large excipients by geometric mixing [14,15]. In the case of water soluble drugs that are poor, the adsorption of small drug particles on the surface of large excipients can expand the dissolution rate by increasing drug surface area and converting drug from crystalline form to the amorphous form [16,17]. Adsorption on the surface has also been involved in other pharmaceutical applications such as drug oxidation [18] granulation of oily medicine [19,20] and some special formulation designs [21,22].

The adsorption exhibited by adsorbents proceeds best from dilute solution, and the adsorbates can either be a gas or liquid [23–25]. The driving force behind adsorption is the formation of bonds between the adsorbate and the solid surface [26], which contains narrow pores which are more effective than globular openings, which encourages the release of heat. We can classify adsorption as a physical or chemical reaction in nature, when they are gaseous condensation, physical adsorption occurs when a solid adsorbent is used in conjunction with a liquid adsorbate in the presence of Van Der Waals forces [27]. Chemical adsorption involves gases adhering to solid surfaces by a combination of chemical forces that are specific to each surface and gas. Adsorption occurs chemically at higher temperatures than physical adsorption. Chemical adsorption is a slower process than physical adsorption and most chemical reactions, involves an activation energy [28]. Therefore, in this study we synthesized a combination of eggshell/bentonite and to improve its adsorption abilities, we changed the mixture combination with $Fe(acac)_3$ to form iron based (IB) nanoparticles. However, humans and the food industry consume eggs as one of the excellent sources of protein, which causes an enormous amount of eggshells to be produced every day as waste [29]. Historically, this waste was discarded without pre-treatment in landfills because it was relatively useless. It was discovered in food processing that the eggshell is high in nutrients like calcium, magnesium, and phosphorus [30,31], and with time, was used as a fertilizer, a soil conditioner, or a feeding additive in agriculture [32–34]. The calcified eggshell contained abundant intrinsic pores, which makes it thus possible to grind eggshells into fine powders, which may lead to materials such as porous adsorbents being developed. Eggshell is one of the most useful adsorbents for removing pharmaceuticals from aqueous solutions used in water treatment [35–37].

One of the most widely used adsorbents among these clays is bentonite because it has a net negative surface charge, making it effective in removing cationic compounds [38]. The bentonite I prepared consists of two tetrahedral sheets of silica fit in between two octahedral sheets of alumina. Isomorphous substitutions of Al^{3+} cause this negative charge in bentonite for Si^{4+} and Mg^{2+} for Al^{3+} at the tetrahedral level. Negative charges in the structure are balanced by exchangeable cations (Na^+, Ca^{2+}, etc.) which enable cationic adsorption of contaminants [39,40]. Therefore, the mixture combination of eggshell, iron (metal) and bentonite was effective for raising the adsorption capacity.

Pharmaceutical removal using iron-based adsorption (IB) is a more recent treatment technique, but it is one of the best ways to remove drugs. Various products have been developed because of this process, including granular ferric hydroxide, zero-valence iron, iron coated sand, and iron oxide based adsorbents [41–43]. As a result of recent advances in nanoscience and nanotechnology, several nanoparticles are being developed to treat various groundwater contaminants [44]. Since nanoparticles have a large surface area and high reactivity, they are suitable for the removal of contaminants from aqueous solutions [45]. This study investigates the efficacy of iron/eggshell/bentonite (FEB) and eggshell/bentonite (EB) to remove acetaminophen dissolved in aqueous solution.

2. Experimental methods

2.1. Synthesis of material

The starting materials employed to synthesize the mixture of iron, eggshell and bentonite (FEB) and the mixture of eggshell and bentonite (EB) nanocomposite. FEB materials are iron (III) acetylacetonate hydrate (99.9% purity) bentonite (carbon) (99% purity) and pluronic F-127 (bioreagent, suitable for cell culture) mixed with eggshell. These chemicals were purchased from Sigma-Aldrich (Pty) Ltd and were used without further purification. Eggshell (calcium) (80%), the eggshell was made naturally by boiling, then washing the eggshells with water and then drying it for 7 d with heat or under the sun. It was then ground in a solid blending machine to powder. The eggshell powder was then mixed up with bentonite (carbon) (99% purity) and pluronic F-127 (bioreagent, suitable for cell culture) to form EB nanocomposite.

2.2. Characterization of adsorbents

To investigate the morphology of the material and measure the particle size scanning electron microscopy (SEM)

was conducted employing an FEI Quanta 250 FEG SEM with an integrated Oxford X-map 20 EDS system. The samples were coated with carbon before examination. N_2 adsorption-desorption was done using the Tri-Star II3020 V1.03 to find the surface area, pore size, pore volume, and the pore size distribution of the original materials. The samples were degassed using the degassing instrument at 90°C for 1 h and 200°C for 5 h. The samples were then analysed with a Tristar II3020 V1.03 using nitrogen at 77 K temperature. Furthermore, X-ray diffraction (XRD) pattern was analysed by using a Siemens D8 Advance diffractometer with a CuKα radiation source operating at 40 kV with a wavelength of 1.5406 Å. The thermogravimetric analysis (TGA) of the samples were measured by heating the samples in air at 30 mL min^{-1} from 30°C to 1,000°C at 10°C/min.

2.3. Procedure for the synthesis of FEB

The synthesis of the material was carried out by utilising 5 g of Fe $(acac)_3$, 5 g of eggshell, and 5 g of bentonite nanocomposite. 8.00 g of pluronic F-127 was weighed into 100 mL of ethanol and after that mixed for 20 min at 180 rpm. The metal ($Fe(acac)_3$) and eggshell ($CaCO_3$) were weighed out independently and mixed in 100 mL of ethanol. Bentonite was then included in 70 mL of Milli-Q water and mixed for 10 mins with a stirrer. The Bentonite mixture was then added to the 100 mL of ethanol and mixed at 300 rpm and 100°C for 14 h until it formed a gel. The material mixture was then dried in an oven overnight at 140°C, and it was calcined in a muffle furnace for 5 h at a ramping rate of 2°C/min, up to the last temperature of 1,000°C.

2.4. Synthesis technique for EB

A combination of eggshell and bentonite was synthesized by utilising 5 g of eggshell, and 5 g of bentonite nanocomposite. The eggshell was weighed into 100 mL of ethanol and after that mixed for 20 min at 300 rpm. Bentonite was poured in 70 mL of Milli-Q water and stirred for 20 min and after that bentonite was poured into the 100 mL of ethanol to mix with the eggshell at 300 rpm and 100°C for 15 h to form a gel. The gel was put in an oven to dry, at a temperature of 140°C for 24 h. The materials were calcined in a muffle furnace for 5 h at a ramping rate of 2°C/min, up to a temperature of 1,000°C.

2.5. Adsorbate preparation

The stock solution of acetaminophen was prepared by pouring 0.1 g of acetaminophen in 1,000 cm^3 volumetric flask. Deionised water was then added to the volumetric flask to dilute the solution up to the mark of 1,000 cm^3. The dilution of this stock solution yielded a working solution of desired concentrations.

2.6. Batch adsorption studies

The removal of acetaminophen was done through batch adsorption process on FEB and EB adsorbents. The processes of pH, contact time, adsorbent dose, initial metal ion concentration, was utilised to investigate the experiments. Experiments were performed sequentially to acquire the worthiest experimental procedure for the adsorption of acetaminophen from aqueous solutions. For the experiment effective solutions of the adsorbent concentrations of 20–100 mol L^{-1}, respectively, were prepared from the stock solutions. Delivery of the adsorption experiments was carried out by pouring 25 cm^3 aliquots of acetaminophen solution into 50 cm^3 polypropylene plastic vials, and changed to achieve the desired pH with appropriate amounts of 0.1 mol L^{-1} NaOH or HNO_3 solution added to it. Time experiment was carried out by agitating 25 cm^3 of the known concentration of acetaminophen solution with 40 mg of adsorbent at a temperature of 25°C for 5 and 18 h in stoppered rubber bottles. The quantity of metal ion adsorbed on each sorbent was estimated from the difference between the initial and equilibrium metal ion concentrations. The adsorption capacity (q_e) and adsorption efficiency (% adsorbed) was calculated from Eqs. (1) and (2) [46].

$$\%\ \text{adsorbed} = \left(\frac{C_i - C_{\text{eq}}}{C_i}\right) \times 100 \tag{1}$$

$$q_{\text{eq}} = \left(\frac{C_i - C_{\text{eq}}}{m}\right) \times V \tag{2}$$

2.7. Analysis of kinetic models

We studied the kinetic effects of acetaminophen with an adsorbent dosage of 40 mg in 25 cm^3 aliquots by unsettling 100 mol L^{-1}, acetaminophen. The blends were set in an orbital shaker at 25°C and unsettled for distinctive time intervals within the stretch of 5–360 min. The acetaminophen equilibrium concentration was determined by gravity filtration and UV-Vis spectrophotometer after a predetermined time interval. Experiments were done to evaluate the pseudo-first, and pseudo-second-order models. The parameters are represented as q_t, quantity of adsorbate adsorbed at time t (mg g^{-1}); q_{eq}, quantity of adsorbate adsorbed at equilibrium (mg g^{-1}); α, adsorption rate constant (mg g^{-1} min^{-1}); β, desorption rate constant (g mg^{-1}); k_1, pseudo-first-order rate constant (min^{-1}); k_2, pseudo-second-rate constant (g mg^{-1} min^{-1}); k_p, intraparticle diffusion rate constant (mg g^{-1} $min^{0.5}$); C, is a constant related to the boundary layer thickness (mg g^{-1}).

2.8. Analysis of isothermal models

Adsorption isotherms were examined by utilizing varying acetaminophen concentrations, extending from 10 to 100 mg L^{-1}, at a consistent pH of 7. Aliquots of 25 cm^3 were mixed with 40 mg of the adsorbents and agitated on an orbital shaking bath under varying temperatures of 293, 303, 313 and 318 K for 2, 6 and 18 h. The UV-vis spectrophotometer experiment was used to filter the gravity and concentrations of acetaminophen pharmaceutical within the filtered arrangements. Six adsorption isotherm models comprising both two-parameter models, Langmuir, Freundlich, Temkin and Dubinin–Radushkevich examined the exploratory adsorption harmony information and the three-parameter models are Sips and Redlich–Peterson models.

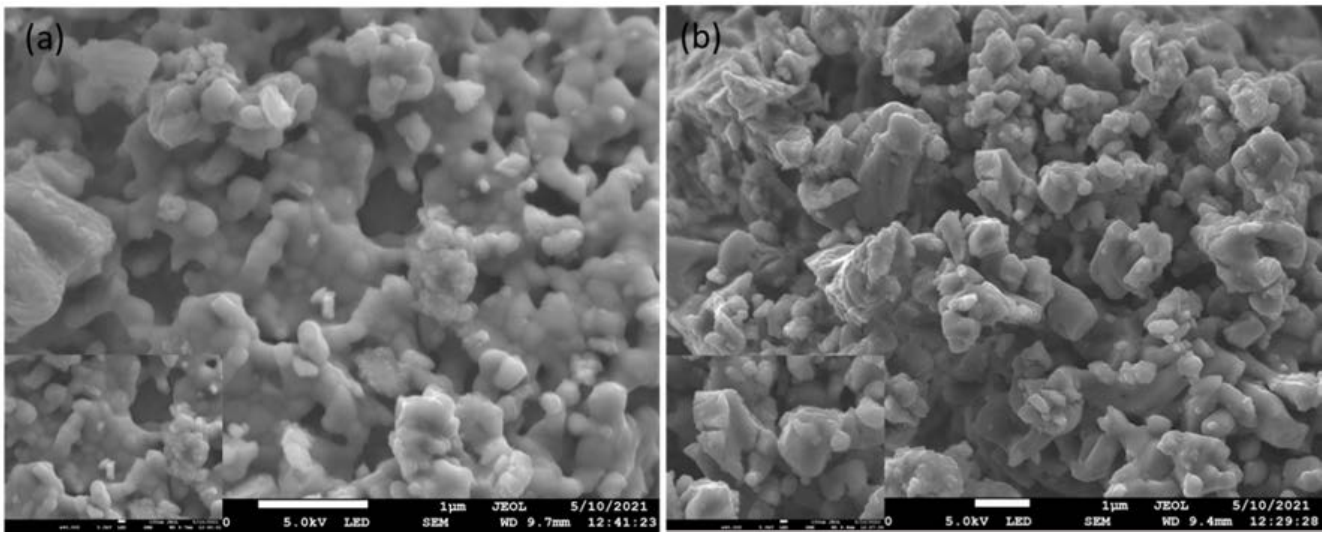

Fig. 1. SEM images of (a) FEB and (b) EB nanocomposites.

The conditions of the models are given in Table 2. Thermodynamic parameters such as a change in Gibbs energy (ΔG), change in enthalpy (ΔH), and change in entropy (ΔS) were also calculated over the studied temperature range. Parameters shown in Table 2 are represented as q_e is adsorption capacity (mg g^{-1}); C_{eq} is the equilibrium concentration of adsorbate in solution (mg dm^{-3}); $q_{m'}$ is maximum monolayer capacity (mg g^{-1}); b is Langmuir isotherm constant (dm^3 mg^{-1}); K_F is Freundlich isotherm constant (mg g^{-1})(dm^3 $mg^{-1})^n$; n is adsorption intensity; b_T is Temkin isotherm constant; A_T is Temkin isotherm equilibrium binding constant (dm^3 g^{-1}); b is Dubinin–Radushkevich isotherm constant (mol^2 kJ^{-2}); is Redlich–Peterson isotherm constant (dm^3 g^{-1}); A is Redlich–Peterson isotherm constant; g is Redlich–Peterson isotherm exponent.

2.9. Desorption analysis

Furthermore, the adsorption test was accomplished with a 50 mol L^{-1} solution of acetaminophen and by adding a 40 mg dosage of each adsorbent. The stacked adsorbents were isolated from the delays by filtration and the metal particle concentration within the filtrates by utilizing the appropriate portrayed procedures. The collected sorbents were washed with deionized water which was used to dismiss unabsorbed metal particles and dry in a vacuum oven at 80°C. The Desorption tests was at this point conducted by unsettling 40 mg of the adsorbent with 25 cm^3 of 0.1 mol L^{-1} HCl for 30 min. The blend was at that point sifted and the concentration of the desorbed metal particles within the filtrates was decided as portrayed some time recently. The percentage of metal desorbed was calculated from Eq. (3):

$$\text{Percentage desorption}(\%) = \frac{\text{Released ion concentration}}{\text{Initial ion concentration}} \times 100 \quad (3)$$

2.10. Data analysis

The information gotten were fixed to the isotherm and kinetic models which implies the nonlinear regression schedule (nls) within the *R* measurable computing environment. The *R* statistical computer program takes into consideration the minimization of the entirety of the adjusted R^2 squared.

3. Results and discussions

3.1. Characteristics of adsorbents

3.1.1. SEM analysis

The FEG-SEM was used to study the morphology of eggshell and bentonite (EB) and then $Fe(acac)_3$ nanocomposite

Table 1
Kinetic models inspected for the adsorption of acetaminophen on FEB and EB

Model	Equation	Parameters	References
Lagergren pseudo-first-order	$\ln(q_{eq} - q_t) = \ln q_{eq} - k_1 t$	$q_{eq'}$ k_1	[47,48]
Pseudo-second-order	$\frac{t}{q_t} = \frac{1}{k_2 q_{eq}^2} + \frac{1}{q_e} t$	$k_{2'}$ q_{eq}	[47,48]

Table 2
Isotherm models explored for the adsorption of acetaminophen on FEB, and EB nanocomposites

Isotherm model	Equation	Parameters	References
Langmuir	$\frac{1}{q_{eq}} = \left[\frac{1}{q_m K_L}\right]\frac{1}{C_{eq}} + \frac{1}{q_m}$	q_m, b	[49]
Freundlich	$\log\left(q_{eq}\right) = \log\left(K_F\right) + \frac{1}{n_f}\log\left(C_{eq}\right)$	K_F, n	[50]
Temkin	$q_{eq} = \frac{RT}{b_T}\ln C_{eq} + \frac{RT}{b_T}\ln A_T$	b_T, A_T	[51]
Dubinin–Radushkevich	$\ln q_{eq} = \ln q_m - \beta\varepsilon^2$ $\varepsilon = RT\ln\left(1 + \frac{1}{C_{eq}}\right)$	q_m, β	[52]
Sips	$\frac{1}{q_{eq}} = \frac{1}{q_m K_s}\left(\frac{1}{C_{eq}}\right)^{1/n} + \frac{1}{q_m}$	q_m, K_s, n	[53]
Redlich–Peterson	$\ln\left(\frac{C_{eq}}{q_{eq}}\right) = \beta\ln C_{eq} - \ln A$	β, A	[54]

was added to the compositional mixture of eggshell and bentonite to form a nanocomposite (FEB). However, these nanocomposite materials were examined to be combined in an agglomerate formation, with open pores that vary in sizes between the different nanocomposites. The SEM morphology of EB displayed the most noteworthy molecule measured to the extent of 52–254.0 nm, taken after by FEB with molecules measuring from 47 to 249 nm. Due to their high calcination temperatures and aggregation following heat treatment, the FEB nanocomposites and EB composites were observed to have large particles.

The energy-dispersive X-ray spectroscopy (EDX) analysis shows that the eggshell contains the key metal of calcium, from ($CaCO_3$) crystals, 3% magnesium and traces of silicon, aluminium and 10% of iron for FEB sample. The eggshell is made up of calcium carbonate crystals and is semipermeable, so moisture and air can pass through it. The shell also has a thin outmost coating called the bloom or cuticle that helps keep out bacteria and dust. Results from EDX analysis (measured weight %) are represented in the below (Table 3), from which the elemental composition was determined for FEB and EB as derived by the instrument.

3.1.2. TGA analysis

Fig. S1 shows the thermogravimetric analysis of the samples calcined at 1,000°C. FEB nanocomposites showed a fast weight loss from 30°C to 400°C and EB also showed a fast weight loss of 19°C–400°C, this is because carbon dioxide desorption occurs. However, there was a gradual weight loss for FEB and EB nanocomposites from 400°C to 580°C because of the desorption of physically absorbed water, and a gradual weight loss showed for FEB from 550°C–900°C and a small weight decrease throughout the process. For EB there were no weight changes, the reaction and consumption of the sample was in equilibrium. The weight changes of the samples were assumed to be mainly because of the behaviour of lattice oxygen as shown by the equations [55,56]:

$$2Fe_{fe}^{oo} + O_O^X \rightarrow 2Fe_{fe}^X + V_o^{oo} + \frac{1}{2}O_2 \quad (4)$$

$$2Ca_{ca}^{oo} + CO_O^X \rightarrow 2CaCO_{ca}^X + V_o^{oo} + \frac{1}{2}O_2 \quad (5)$$

$$2CoO_{co}^{oo} + O_O^X \rightarrow 2COO_{co} + V_o^{oo} + \frac{1}{2}O_2 \quad (6)$$

where V_o^{oo} and O_O^X represent oxide ion vacancy and oxide ions, respectively. The reduction reaction was nearly the same for eggshell/bentonite and FEB samples calcined at 1,000°C because of its gradual weight loss throughout the process [57]. This is as a result of thermal-induced lattice oxygen loss caused by the increase in oxygen vacancies formation complemented by a change in the valence of Ca and Fe ions from IV to III to maintain electrical neutrality. This causes a shift in the equilibrium positions of Eqs. (5) and (6) to the right accompanied by a weight reduction. Furthermore, the starting temperature for lattice oxygen loss was earlier in the samples calcined at 1,000°C.

In conclusion, the samples showed high thermal stability and thermal reduction of the materials started occurring at lower temperatures and faster with limited weight loss at higher calcination temperatures; hence the material is suitable for adsorption.

3.1.3. Fourier-transform infrared spectroscopy analysis

The Fourier-transform infrared spectroscopy (FTIR) in Fig. S2 shows the stretching vibration mode of the O –H bond at 3,643.2 and 3,640.75 cm^{-1}, while the broadband seen at 2,848.6–2,919.7 cm^{-1} corresponds to C–O. Peaks at 1,480; 1,414 and 1,482.6 cm^{-1} for FEB indicate the presence of free water molecules connected by an O–H bond. Furthermore, some peaks were also seen at 1,049 and 1,154 cm^{-1}, for EB, which represents a Si^{4+}–O intermediate or resonance structure Al^{3+}–O, and implies possible bridged superoxide intermediates such as [Ca^{2+}–(OO)–Ca^{2+}] [58,59]. There is also a tension mode associated with a COO-monodentate coordination compound, which eventually moves to lower frequencies, and these modes are also related [60]. Peaks were noticed at 900.1 and 901.46 cm^{-1}, which represents the bonding of O_2 and OH with the distinctive metal cations of Fe^{3+} and Ca^{2+} corresponding to the vibrational modes of (O–C–O) and (C–OH) [61,62]. The peaks also represent spinel metals (Fe^{3+}) in the nanocomposite.

3.1.4. XRD analysis

The EB and FEB nanocomposites were characterized using XRD and Rietveld refinement analysis. Fig. S3 shows the XRD profiles for the diffraction peaks for EB and FEB nanocomposite, (Fig. S3a) shows 6 phases which are calcium hydroxide ($Ca(OH)^2$) phase seen at 18.07°, 28.579°, 30.032°, 47.10°, 50.83°, 52.15°, 62.61°, 64.184°, 71.76° were indexed to (001) (110) (119) (102) (110) (300) (021) (013) and (022). CaO (calcium oxide) phases can be seen at 32.19, 37.24, 53.95 and 64.18 which were indexed to (111) (200) (220) and (311). $2Ca_4Fe_{14}O_{25}$ (calcium iron oxide) phase seen at 29.79°, 30.03°, 35.56°, 39.17°, 46.85°, and 52.16° indexed to (113) (119) (0210) (111) (122) (222) and (300). Fe_2O_3 (maghemite) phase at 35.56°, 39.17°, 49.50°, 54.08°, 56.49°, 57.08°, 62.50° and 63.94° were indexed to (110) (006) (024) (116) (211) (122) (214) (300). $2CaO.SiO_2$ phase at 23.89°, 31.22°, 32.31°, 33.04°, 39.16°, 46.85°, 47.10° was indexed to (102) (013) (020) (013) (203) (302) and (204). Ca_2SiO_4 (calcium silicate) phase seen at 18.01°, 22.09°, 23.89°, 27.86°, 28.57°, 29.79°, 31.35°, 32.19°, 34.12°, 35.56°, 36.64°, 37.24°, 39.29°, 41.21°, 42.30°, 44.33°, 45.66°, 47.10°, 50.83°, 51.92°, 52.16°, 54.08°, 56.49°, 57.08°, 60.82° and 64.18° indexed with (–101) (–111) (111) (–211) (120) (211) (021) (–301) (301) (012) (–202) (112) (–212) (130) (022) (–312) (411) (420) (510) (013) (–132) (132) (520) (213) (224) and (215). $K_2Ca(CO_3)_2$ (potassium calcium carbonate) phase was seen at 33.03°, 33.87°, 39.29°, 41.21°, 53.95°, and 71.76° are indexed to (104) (110) (200) (202) (116) (220). $KAl_3(SO_4)_2(OH)_6$ (potassium aluminium sulfate hydroxide) phases seen at 25.45°, 31.35°, 36.64°, 39.29°, 44.33°, 47.10°, 52.15°, 62.61°, and 71.76°, which is indexed to (110) (006) (024) (107) (214) (033) (220) (0210) and (410). MgO (manganese oxide) phases were seen at 36.64, 42.30, and 62.50, which is indexed to (111) (200) (220). The nano-composites materials possessed lattice parameters of Rhombohedral, "a" is 5.0356 Å, molecular weight (MW) of 159.9, volume (CD) of 301.93 cm^2 and density (Dx) is 5.270 g cm^{-3} for Fe_2O_3. The lattice parameters are monoclinic, "a" is 9.3100 Å, the MW is 172.24, and CD of 345.29 cm^2 and Dx is 313 g cm^{-3} for Ca_2SiO_4. For calcium iron oxide ($Ca_4Fe_{1.4}O_{25}$) the lattice is rhombohedral, "a" is 6.0000 Å, molecular weight is 1,342.16, volume (CD) is 2,961.81 cm^2 and density (Dx) is 0.752 g cm^{-3}. The lattice parameter for $CaMgS_{12}O_6$ is monoclinic, "a" is 5.0356 Å, MW is 216.55, CD is 439.50 cm^2 and Dx is 3.273 g cm^{-3}. For anhydrite ($Ca(SO_4)$), the lattice is based centred orthorhombic, a is 6.9910 Å, MW is 136.14, CD is 305.09 cm^2 and Dx is 2.964 g cm^{-3}. $KAl_3(SO_4)^2(OH)_6$ has a lattice of rhombohedral, a is 6.9979 Å, MW of 414.20, CD of 725.84 cm^2 and Dx of 0.948 g cm^{-3}, the nanomaterial called MgO which showed a lattice of Face centred cubic structure (space group: Fm3m) with "a" as 4.2112 Å, the MW is 40.30, CD is 74.68 cm^2 and Dx is 3.585 g cm^{-3}. For the case of EB nanocomposite some components such as CaO shows a face centred cubic lattice with "a" is 4.81105 Å, and MW of 56.08, a CD of 111.33 cm^2, and a Dx of 3.346 g cm^{-3}. Also for the $Ca(OH)_2$ phase, the lattice is hexagonal, "a" is 3.5890 Å, MW is 74.09, CD is 54.78 cm^2 and Dx is 2.246 g cm^{-3}. The values of "a" for all the phases of the samples, calcined at 1,000°C respectively looked very similiar. The Bravais lattice for the phases of the sample was calculated using Eq. (7).

$$a = \frac{\lambda}{2} \wedge \sin\theta \wedge \sqrt{h^2 + k^2 + l^2} \tag{7}$$

where λ is the average X-ray wavelength, θ is (2θ value/2), and *hkl* represents the Miller's indices of the particular planes in the crystal. The density values are calculated using this equation.

$$\text{Density} = \frac{\text{mass}(\text{unit cell})}{\text{Volume}(\text{unit cell})} \tag{8}$$

3.1.5. Brunauer–Emmett–Teller analysis

Physical adsorption of a gas on the surface of a solid determines its specific surface area, as well as the amount of gas adsorbing on a monomolecular layer on the surface. Volumetric or continuous flow procedures can determine the amount of gas adsorbed. The isotherm plot of the samples is shown in Fig. 2, and the textural properties of the samples have been scanned with the nitrogen desorption analysis as shown. The isotherm plot shows that the materials are type III isotherms, which showcases a macroporous material that is observed at the diameter of the spherical pores and slit pores within distances between opposite walls.

The pores of these sizes could safely transport ions and electrons. The surface area was 2.482 m^2 g^{-1}, and the pore volume of 0.3959 cm^3 g^{-1} were possessed by the EB sample calcined at 1,000°C. While the surface area for the FEB sample, the iron mixture eggshell calcined at 1,000°C was 2.116 m^2 g^{-1}, with a pore volume of 0.7779 cm^3 g^{-1}. The observations show that $Fe(acac)_3$ addition and mixture increased

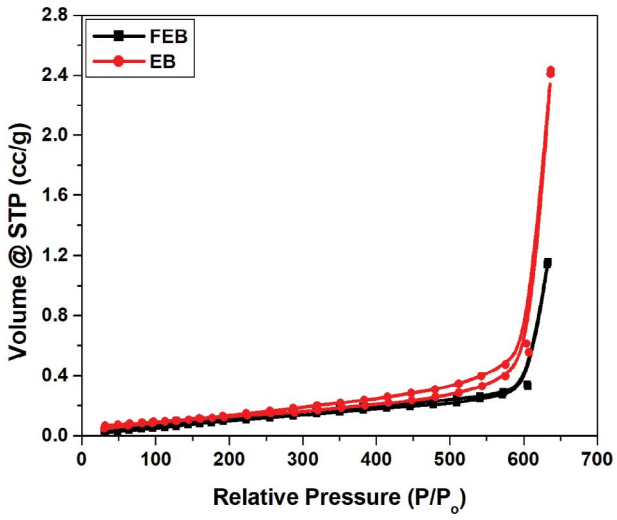

Fig. 2. The Brunauer–Emmett–Teller analysis of FEB and EB nanocomposites calcined at 1,000°C for 5 h.

the eggshell pore volume. The surface area of the materials was low and the material surfaces had a tendency to decrease with the increase in calcination temperature. This is likely due to the fact that the higher the temperature, the more compact the material becomes. In addition, the particles might agglomerate if the temperature is increased too quickly, resulting in a low surface area.

3.2. Experiments with batch adsorption

The adsorbents such as iron/eggshell/bentonite (FEB) and eggshell/bentonite (EB) were used for the adsorption of acetaminophen which were examined for the effective remediation of polluted wastewater. Furthermore, adsorbents were examined for their adsorption capacities to determine which is most effective for evacuation of pharmaceuticals. In addition, we adapted pH, contact time, initial pharmaceutical concentration, temperature, and adsorbent dosage to achieve the optimum conditions required for pharmaceutical removal without polluting the environment.

3.2.1. Effect of pH

The effect of pH on the removal of acetaminophen from aqueous solution by the mixture eggshell/bentonite (EB) powder and the addition of $Fe(acac)_3$ to EB powder (FEB sample) was studied at various pH values (ranging from 2–10). It has been written that the 40 mg dosage of adsorbents pH of solution affects the surface charge of the adsorbent material. It is also forwardly related with the competition capacity of $[H^+]$ and adsorbate particles on the active sites of the adsorbent surface.

The removal of acetaminophen by the adsorbents was well-known to increase with increase in pH of the adsorbate solution appreciably up to pH 6.0 (Fig. 3). Salleha et al. state that cationic adsorption is ideal when the pH of the solution is superior to the point of zero charges (pH_{PZC}). This statement can be identified in these results illustrated in Table 3, the measurement of pH_{PZC} values were lower than the optimum pH condition which were obtained for all the absorbents. The attractive interaction between the acetaminophen charges and the negatively charged adsorbent surface is in charge of adsorption.

3.2.2. Effect of contact time

As shown in Fig. 4 in this case, acetaminophen was studied for adsorption within the time range of 5–360 min. The initial concentration (100 mg dm^{-3}), pH and adsorbent dose (40 mg) were maintained during the process. The results of the study indicate that the percentage removal of pharmaceutical increased with time and that an equilibrium was achieved for FEB at 210 min and an

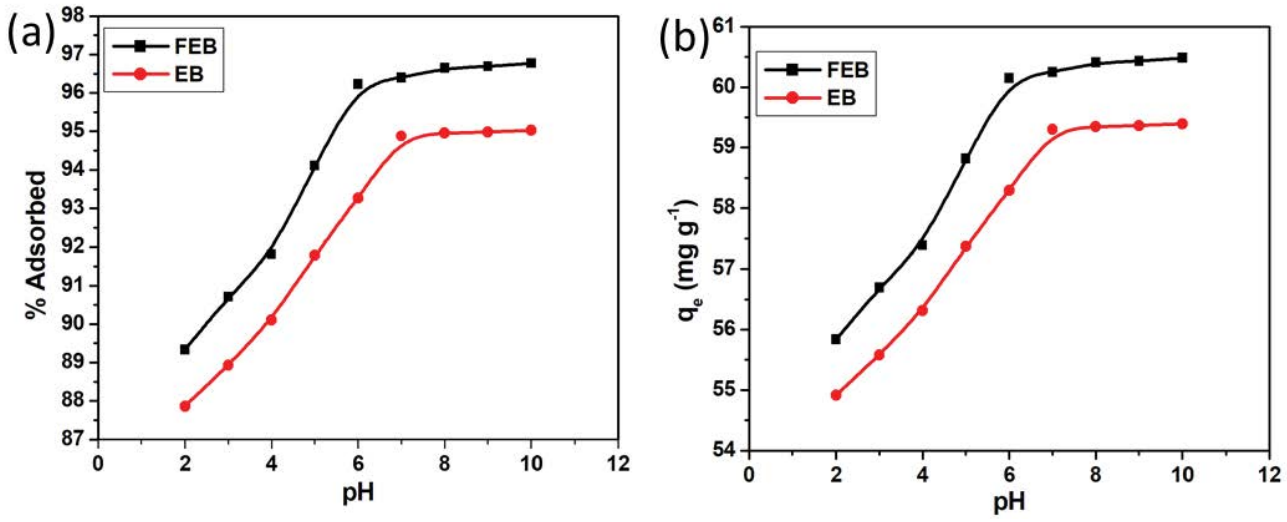

Fig. 3. Effect of pH on the adsorption of acetaminophen onto FEB and EB adsorbents [conditions: 25 cm^3 of 100 mg dm^{-3} of acetaminophen, 18 h equilibration time, adsorbent dose, agitation speed 150 rpm, temperature 25°C].

equilibrium for EB at 180 min. During this stage, the percent adsorption remained constant with little or no further increase official destinations on the surface of the adsorbents were possessed, the encouraged expulsion of acetaminophen was watched to be negligible. Despite both adsorbents having quick adsorption times, FEB exhibited a higher expulsion rate than EB when tested. Possibly, this is due to the fact that an impressive number of chelating sites are formed by the functionalization of iron by the eggshell and bentonite compounds. However, the greatest time for mixing was blended at 6 h to discover the total evacuation of acetaminophen from fluid mixture beneath all conditions [63].

3.2.3. Adsorption kinetics

Adsorption kinetics are extremely essential for deciding the efficiency of the adsorption process for the uptake of acetaminophen on the surface of FEB and EB nanocomposites. This in turn controlled the residence time at the solid solution adsorbent interface. For this reason, it is important to predict the absorption rate for the removal of acetaminophen from the water effluents. Therefore, this was investigated by using Lagergren pseudo-first-order [41], and pseudo-second-order [64]. However, the equations used for these models are represented in Table 2, these equations were applied for the adsorption of acetaminophen on the combination eggshell powder and other metals. In addition, the pseudo-first-order kinetic model was used to predict the sorption of acetaminophen kinetics and the pseudo-second-order is a chemisorption kinetics rate for adsorption. This is the dissemination of adsorbates from the bulk solution onto the adsorbent surface, and the sanctioning of adsorbates through the fluid film onto the adsorbent surface (film dissemination), [65]. This can be a certainty of the model to be used to best fit the experiment with a linear regression analysis graphically close to/or 100% for a chart squared residual (R^2).

The R^2 values decided by direct relapse investigation are displayed in Table 4. The R^2 esteem of the pseudo-second-order kinetic model are a great deal higher than other models. Table 4 shows that the estimates of the kinetic model information gotten are best portrayed by the

Table 3
EDX analysis for SEM images of (a) FEB and (b) EB nanocomposites

Element	FEB	EB
	Weight %	Weight %
Carbon (C)	18.2	40.7
Oxygen (O)	27.7	27.5
Magnesium (Mg)	0.5	0.4
Aluminium (Al)	2.3	0.5
Silicon (Si)	7.2	1.0
Calcium (Ca)	34.4	29.7
Iron (Fe)	9.6	–
Total	100.0	100.0

Table 4
Kinetic parameters for the adsorption of acetaminophen from aqueous solution

Model	Parameters	FEB	EB
Experimental			
Pseudo-first-order	K_i (min^{-1})	0.911E-6	0.817E-6
	q_e (mg g^{-1})	2.629	5.366
	R^2	0.753	0.516
Pseudo-second-order	k_2 (g mg^{-1} min^{-1})	0.004	0.018
	q_e (mg g^{-1})	54.945	50.916
	R^2	0.999	0.999

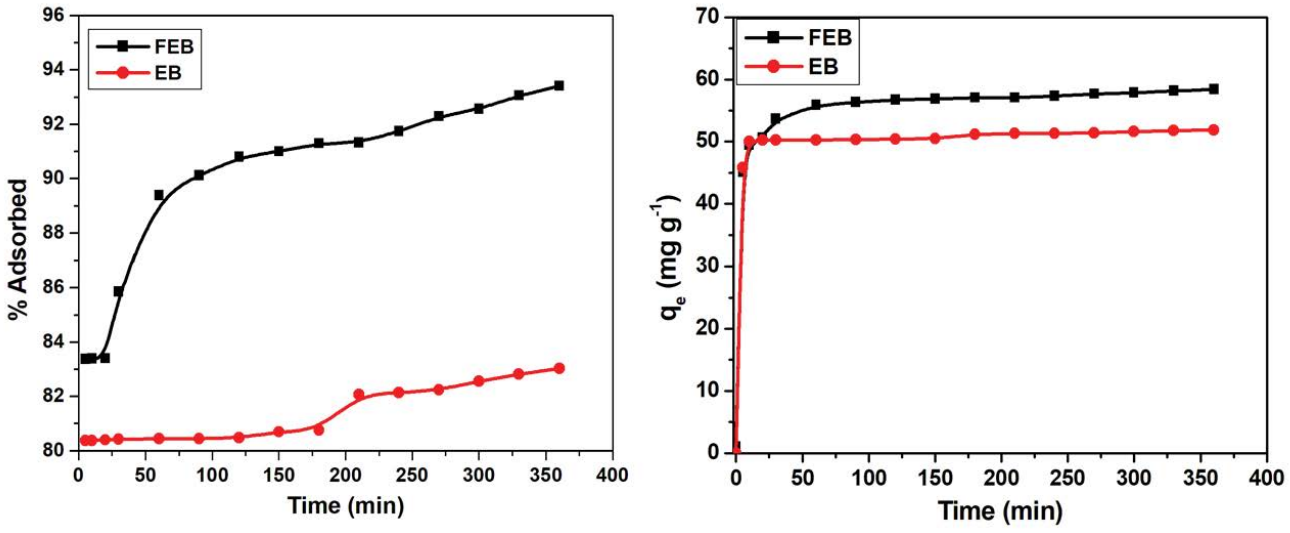

Fig. 4. Effect of contact time on the adsorption of acetaminophen onto FEB and EB adsorbents [conditions: 25 cm^3 of 100 mg dm^{-3} of acetaminophen, 6 h equilibration time, 40 mg adsorbent dose, agitation speed 150 rpm, temperature 25°C].

pseudo-second-order model of EB at (0.999) and (0.999) for FEB which was bigger than the pseudo-first-order model of 0.516 for EB and 0.753 for FEB. In spite of the q_e calculated and the experimental values evaluated using pseudo-first-order model. The values for FEB and EB adsorbent does not match with each other. In the case of pseudo-second-order model, there was a good arrangement with the adsorbents, thus the adsorption of acetaminophen on FEB and EB adsorbent followed pseudo-second-order model [66–68].

3.2.4. Effect of dosage of the adsorbents

Adsorbent mass values ranged between 20 and 100 mg. Nevertheless, as the adsorbent dosage rises and other parameters remain constant, the removal efficiency first increases, then reaches a maximum and then decreases. From the experiment, it was taken note that the increment within the measurements to 100 mg, progressed at 99% removal effectiveness obtained by the adsorbents. As the amount of adsorbent dose increased, the amount of acetaminophen taken up decreased as shown in Fig. 5. Furthermore, the dynamic active sites are higher at lower concentrations of adsorbents which leads to an increment in adsorbent dosage and particle conglomeration. This is attributable to acetaminophen becoming less effective and decreasing in absorption. The capability of adsorbents available for adsorption is majorly improved by the adsorbent's surface area and pore volume. Moreover, at higher adsorbent concentrations, the adsorption capacity is greater for higher surface area materials (larger pore size) due to increasing pore volumes.

3.2.5. Effects of drug concentration

To determine the increment within exercises (q_e) of each adsorbent, distinct concentration ranges with the same amount of adsorbent were used. The outcome of the changes in adsorption efficiency upheld at previous concentrations is presented in Fig. 6. Moreover, the concentrations used were measured from 10–100 mg L^{-1} at 20 mg L^{-1} intervals and 40 mg of the adsorbent was utilised and these parameters were maintained constant. The concentration of adsorbate also increased when the adsorption quantity increased (q_e). The removal efficiency of the adsorbent is shown to be high, which comes from more active sites on the surface area of adsorbent when adsorbate concentration is low. However, the increment in adsorption capacity compared to the increment within the beginning concentration of adsorbate is obtained, resulting from an increment within the driving force due to the concentration slope created between the bulk arrangement and the surface of the adsorbent. Which makes the saturation of the active sites occur with molecules of adsorbate molecules at higher concentrations, in a continual process. Thus, the adsorption rate is reduced as the concentration increases, while acceptance of adsorbate (q_e) by adsorbents is increased.

3.2.6. Effect of temperature

Fig. 6 shows the performance of temperature on the adsorption of acetaminophen on the adsorbents was examined at 298, 308, 318 and 328. Table 5 shows that there was a decrease in the adsorption capability (q_m) of FEB and EB adsorbents at higher temperatures and an increase at lower temperatures for the various temperatures from 298 to 328 K for acetaminophen. The results in this work clearly indicate that the adsorption of acetaminophen on both the FEB and EB adsorbents occurred well at low solution temperatures [68].

The performance of temperature on the adsorption of acetaminophen on the adsorbents was examined at 298, 308, 318 and 328 K. Table 5 showed there was a decrease in the adsorption capability (q_m) of FEB and EB adsorbents at higher temperatures and an increase at lower temperatures for the various temperatures from 298 to 328 K for acetaminophen. The results in this work clearly indicate that

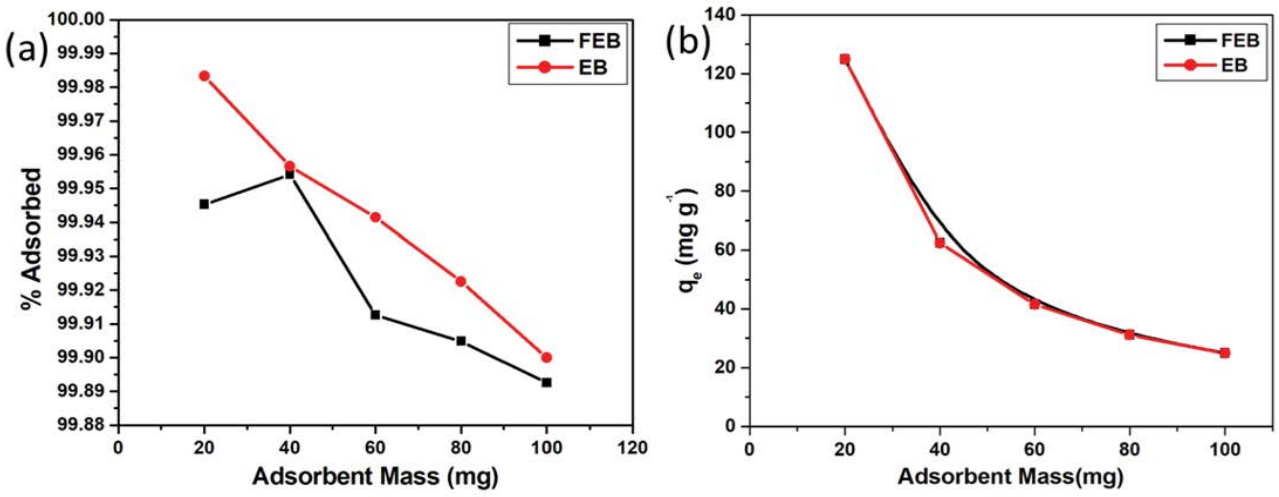

Fig. 5. Effect of adsorbent dose on the adsorption of acetaminophen onto FEB and EB adsorbents [conditions: 25 cm^3 of 100 mg dm^{-3} of acetaminophen, 40 mg adsorbent dose, pH 7, agitation speed 150 rpm, temperature 25°C].

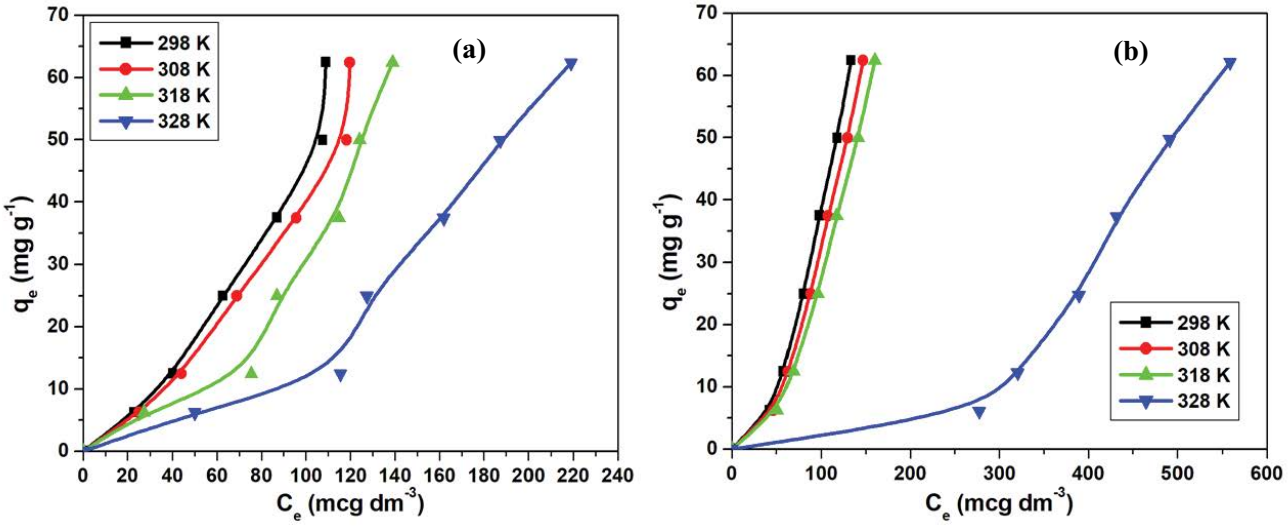

Fig. 6. Effect of temperature on the adsorption of acetaminophen on (a) FEB and (b) EB adsorbent [conditions: 25 cm^3 of 100 mol L^{-3} of acetaminophen, 40 mg adsorbent dose, pH 7, agitation speed 150 rpm, the temperatures are 25°C, 35°C, 45°C, 55°C].

the adsorption of acetaminophen on both the FEB and EB adsorbents occurred well at low solution temperatures [68].

This results can show that the temperature on this adsorption reaction of the acetaminophen molecules in the solution shows that it is crucial. It is observed that according to the adsorption theory, adsorption decreases with increase in adsorbate temperature. The molecules also adsorbed early on the surface tend to desorb from the surface at elevated temperatures and a decrease in diffusion across external boundaries is also caused by an increase in solution viscosity [69,70]. This adsorption process causes acetaminophen, to be accumulated on the surface only, they do not enter through the surface into the bulk of the liquid (a decrease in porosity and pore volume of the adsorbents). This procedure also favoured the uptake of acetaminophen on the surface of the adsorbate which was caused by freedom movement of the adsorbents on the adsorbates. These procedures can suggest that the adsorption can be exothermic in nature.

3.3. Isotherms of adsorption

The capacity of adsorbents and the amount of adsorbents required to get rid of a unit mass of adsorbates are displayed by the models of isotherm. The isotherm models used for this experiment were six. Which includes various two parameter isotherms which are Freundlich [72], Langmuir [73], Temkin, [74], Dubinin–Radushkevich [75], and three-parameter isotherms which are Sips, [76] and Redlich–Peterson, [77]. The models equations are shown in Table 2 and the isotherm model parameters that were calculated during the models experiment are shown in Table 5. The model which showcased the best equilibrium data was the value $R^2 \leq 1$. The equilibrium data results obtained by parameters of the models were summarised for each adsorbent in Table 5. The results showed that Freundlich isotherm best fits the equilibrium data for EB adsorbent. Its application in the adsorption process happens on heterogeneous surfaces and multi-adsorption sites [72]. This describes the surface heterogeneity of the FEB and EB adsorbents as well as the exponential transport of active sites [73]. According to Table 5, the equilibrium data obtained for each adsorbent was best fitted by the parameters of the best model. These outcomes led to the conclusion that Langmuir's isotherm predicted the best adsorption dynamics of monolayers on homogeneous surfaces [73]. Furthermore, it was determined that the best of the two-parameter models considered was the Langmuir and Freundlich Isotherm. As for FEB and EB nanocomposites, the Sips model, which amalgamates Freundlich and Langmuir isotherms, was the best of the three parameter models. This suggests that the uptake of acetaminophen onto the adsorbent sites occurred uniformly, this caused the adsorbate ions not to interact with each other. However, the value K_L shown in (Table 5) indicates how effective the adsorbent is with binding to the adsorbates (i.e., how strong the adsorption is). In the nanocomposites, increasing the amounts of EB increased the adsorptive strength (K_L) (Table 5). Furthermore, this study demonstrates that the acetaminophen and adsorbents formed strong interactions as the EB and FEB contents increased.

3.4. Thermodynamic parameters of adsorption

These thermodynamic parameters were achieved at different temperatures by the quantities adsorbed. The change in Gibbs energy ($\Delta G°$) can be calculated with Eq. (11)

$$\Delta G° = -RT \ln K \tag{9}$$

where $\Delta G°$ represents the standard Gibbs energy change in J mol^{-1}, R represents the gas constant (8.314 J K^{-1} mol^{-1}), T represents the temperature in Kelvin (K) which was achieved from the product of q_m and b obtained from the Langmuir plot (Table 5) [85]. K was achieved dimensionally by multiplying with a factor of 1,000. However, for the

Table 5
Isotherm parameters for the adsorption of acetaminophen onto FEB and EB adsorbents

Adsorbent	Isotherm	Parameters	Temperature			
			298	308	318	328
FEB	Langmuir	q_m (mg g^{-1})	46.339	46.317	90.909	38.139
		K_L (L mg^{-1})	5.238	4.766	2.296	2.748
		R^2	0.999	0.999	0.969	0.976
	Freundlich	n	0.573	0.707	0.715	0.619
		K_F (L mg^{-1})	1.899	20.912	18.089	16.790
		R^2	0.961	0.996	0.947	0.961
	Dubinin–Radushkevich	q_m (mol g^{-1})	191.541	181.363	199.018	141.500
		β (mol kJ^{-2})	3.984E-8	3.859E-8	3.546E-8	4.584E-8
		R^2	0.989	0.989	0.956	0.937
	Temkin	b_T (J mol^{-1})	32.737	32.739	31.301	36.667
		A_T (L g^{-1})	43.033	39.120	35.609	18.476
		R^2	0.933	0.933	0.916	0.885
	Sips	q_m (mg g^{-1})	469.483	476.190	87.719	103.092
		K_s (1 mg^{-1})	2.798	2.333	11.457	8.083
		n	0.707	0.707	0.716	0.619
		R^2	0.998	0.997	0.917	0.927
	Redlich–Peterson	β	0.415	0.415	0.384	0.583
		A	0.001	0.001	0.001	0.002
		R^2	0.955	0.955	0.892	0.928
EB	Langmuir	q_m (mg g^{-1})	16.555	16.543	16.534	6.913
		K_L (L mg^{-1})	6.826	6.206	5.689	1.834
		R^2	0.982	0.982	0.982	0.942
	Freundlich	n	0.293	0.499	0.499	0.299
		K_F (L mg^{-1})	1.283	32.806	30.415	15.192
		R^2	0.987	0.998	0.998	0.987
	Dubinin–Radushkevich	q_m (mol g^{-1})	398.311	365.256	341.757	476.563
		β (mol kJ^{-2})	6.595E-8	6.429E-8	6.266E-8	6.476E-7
		R^2	0.999	0.999	0.999	0.996
	Temkin	b_T (J mol^{-1})	48.129	48.124	48.119	81.965
		A_T (L g^{-1})	23.913	21.738	19.926	3.649
		R^2	0.971	0.971	0.971	0.977
	Sips	q_m (mg g^{-1})	400	400	400	133.333
		K_s (1 mg^{-1})	8.999	8.333	6.253	3.409
		n	0.499	0.499	0.499	0.299
		R^2	0.999	0.997	0.997	0.980
	Redlich–Peterson	β	1.005	0.534	0.534	0.535
		A	0.001	0.001	0.001	0.002
		R^2	0.993	0.959	0.959	0.959

values obtained from the change in enthalpy, ($\Delta H°$) and entropy change ($\Delta S°$) were linked to Van't Hoff equation [85].

$$\ln K = -\frac{\Delta H°}{RT} + \frac{\Delta S°}{R} \tag{10}$$

This equation is connected to the linear plot (graph) of ln$K$ against 1/T which produces the slope ($\Delta H°$) and intercept ($\Delta S°$). Additionally, the change in Gibbs energy generated values that are negative which indicates a spontaneous and feasible nature represented by the adsorption of acetaminophen on the surface area of the adsorbents experimented. In Table 7 it is also shown that the negative values increased as the temperature decreased, which denotes that better adsorption occurs as temperature decreases. Furthermore, the Entropy change produced positive values for all adsorbents which denotes that there is an increase in the degree of system disorderliness with decrease in temperature for FEB and increase

Table 6
Comparison of value findings for acetaminophen by EB and FEB with other methods and/or adsorbents based on the removal capacities, and removal time

Adsorbents	Adsorbate	Concentration (ng L^{-1}, mg L^{-1})	Adsorption capacity (mg g^{-1})	Equilibrium time (min)	References
Waste tea	Acetaminophen	100 mg L^{-1}	195.95	30	[78]
Commercial activated carbon	Acetaminophen	517 mg L^{-1}	221	5	[79]
Moringa oleifera Lam. (seed husks)	Acetaminophen	0.03–9,822 ng L^{-1}	17.48	1080	[80]
Activated carbon in simulated gastric fluid	Acetaminophen	2,500 mg L^{-1}	840	240	[81]
Iron/bentonite/eggshell	Acetaminophen	10–100 mg L^{-1}	469	150	This study
Bentonite/eggshell	Acetaminophen	10–100 mg L^{-1}	400	50	This study
Sugarcane bagasse	Acetaminophen	80 mg L^{-1}	0.32	120	[82]
Corn cob	Acetaminophen	80 mg L^{-1}	0.47	160	[82]
Green horse – chestnut shell	Acetaminophen	10 mg L^{-1}	81	10	[83]
Activated carbon in dilute aqueous solution	Acetaminophen	10 mg L^{-1}	1.077	1200	[83]
MCM-41-GO	Acetaminophen	200 mg L^{-1}	322.6	200	[84]
MCM-41-G	Acetaminophen	200 mg L^{-1}	555.6	220	[84]
ASM41	Acetaminophen	200 mg L^{-1}	121.9	30	[84]

Table 7
Thermodynamic parameters for the adsorption of acetaminophen onto FEB and EB adsorbent

Adsorbent	Temperature (K)	$\Delta G°$ (kJ mol^{-1})	$\Delta H°$ (kJ mol^{-1})	$\Delta S°$ (JK^{-1} mol^{-1})
FEB	298	–15.738	–6.128	32.469
	308	–16.266		
	318	–16.384		
	328	–16.775		
EB	298	–15.234	+4.564	66.248
	308	–15.745		
	318	–16.256		
	328	–17.190		

in temperature for EB. These results exhibits that the adsorption procedure was entropy-driven for all adsorbents in this experiment since an endothermic enthalpy of adsorption was observed for the EB adsorbents and an exothermic enthalpy of adsorption was observed for FEB adsorbent. The interaction on the surfaces of adsorbents can occur through physical interaction (physisorption) or chemical sorption (chemisorption). When the heat of adsorption is between 2.1 to 20.9 kJ mol^{-1}, a physisorption process is assumed to occur while chemisorption could be said to occur when the heat of adsorption is between 80 to 200 kJ mol^{-1} [86]. The ΔH values in Table 6 also indicate that acetaminophen is physisorbed within the surface of FEB and EB nanocomposites.

3.5. Desorption experiments

The experiments for desorption were measured to determine how to reuse adsorbents for testing. This is prepared by using 40 mg of acetaminophen sample with either 10 cm^3 of ethanol or acetone. It is important, it is essential to discover if adsorbents can be regenerated and produced effectively for reuse. In this way the release of auxiliary toxins into the environment is prevented in that the adsorbents are exploited, reused and not disposed specifically after usage. The adsorbate can also be recovered for reuse, after successive adsorption-desorption cycles, a little decrease in adsorption capacity was observed. After four desorption cycles was done, it was shown in the experimental results that good desorption efficiency occurs when ethanol or acetone is used. It was discovered that acetone was better with efficiency within 85%–95%. Furthermore, the reusability was confirmed by characterizing the regenerated adsorbents in this experiment and discovered they are comparative to those gotten with naturally arranged fresh adsorbents, hence confirming its reusability. This shows that the adsorbents used in this experiment are reusable.

3.6. Possible mechanisms of adsorption

To understand the capability of FEB and EB as efficient adsorbents for acetaminophen removal, FTIR analysis was carried out to determine the functional groups present in the adsorbent based on the changes in the vibrational frequencies. The functional group standing for each peaks and stretch are shown in Table 4. The shift in the peak

Table 8
Percentage desorption of acetaminophen by using acetone or ethanol [conditions: 10 cm^3 of either acetone or ethanol, 40 mg of adsorbent, agitation speed 150 rpm, equilibration time 1 h, and temperature 25°C]

Absorbents	Desorption %	
	Acetone	Ethanol
Acetaminophen		
FEB	95.71	85.37
EB	86.53	90.23

from 3,643.2 to 3,640.75 cm^{-1} specified that the stretching of the –OH group was responsible for the binding of Acet ions onto the adsorbent. It was discovered that the resonance structures such as C=O, C–H, Si^{4+}–O, Al^{3+}–O stretch, and Ca^{2+}–(OO) bend were also responsible for the effective removal of Acet ions as it can be elucidated from Fig. S2.

4. Conclusion

We synthesized novel sorbent materials, such as as-synthesised FEB and EB, studied their characterisation extensively, and used them to adsorb acetaminophen, a dominant emerging pollutant. The impact of retaining the surfactant template within FEB and EB was studied and also the synergistic adsorption resulting from the encapsulation of FEB and EB for the adsorption of acetaminophen was also studied. The improved adsorptive capability of the adsorbents grew as a result of increased hydrophobicity by the retention of the F127 template on the adsorbents. In the course of the adsorption process, equilibrium was reached within less than 180 min. A pseudo-second-order adsorption kinetic model fit the data and for two-parameter model Langmuir, and for three-parameter model Sips had the best fit for the isotherm. As a result of the synergistic action of the two molecules species, acetaminophen was removed more effectively by FEB and EB, electrostatic interactions and hydrophobic interactions were involved in adsorption. The adsorption capacity of EB was 16.55 mg g^{-1} and FEB 46.34 mg g^{-1} for the removal of acetaminophen pharmaceutical at 25°C. However, separation from the aqueous phase was made better with the help of iron metal, which worked to prevent agglomeration. On the other hand, a variety of carbon and oxygen surface functional groups were introduced by eggshell and bentonite, considerably increasing adsorption. The thermodynamic findings discovered the adsorption process as spontaneous and exothermic in nature. Regeneration studies showed that adsorbents were reusable for other applications. On real samples of water, the adsorbents performed well, thus making them suitable for removing pharmaceuticals from fluids.

Acknowledgements

The authors gratefully acknowledge the financial support received from the National Research Foundation, South Africa (Grant No: 120668), and the Research Directorate of the University of South Africa, Florida Campus.

Symbols

q_t	—	Quantity of adsorbate
t	—	Time, mg g^{-1}
q_{eq}	—	Quantity of adsorbate adsorbed at equilibrium, mg g^{-1}
α	—	Desorption rate constant, mg g^{-1} min^{-1}
β	—	Desorption rate constant, g mg^{-1}
k_1	—	Pseudo-first-order rate constant, min^{-1}
k_2	—	Pseudo-second-rate constant, g mg^{-1} min^{-1}
k_p	—	Intraparticle diffusion rate constant, mg g^{-1} $min^{0.5}$
C	—	Constant related to the boundary layer thickness, mg g^{-1}
q_e	—	Adsorption capacity, mg g^{-1}
C_{eq}	—	Aquilibrium concentration of adsorbate in solution, mg dm^{-3}
q_m	—	Maximum monolayer capacity, mg g^{-1}
b	—	Langmuir isotherm constant, dm^3 mg^{-1}
K_F	—	Freundlich isotherm constant, (mg g^{-1}) $(dm^3\ mg^{-1})^n$
n	—	Adsorption intensity
b_T	—	Temkin isotherm constant
A_T	—	Temkin isotherm equilibrium binding constant, dm^3 g^{-1}
b	—	Dubinin–Radushkevich isotherm constant, mol^2 kJ^{-2}
A	—	Redlich–Peterson isotherm constant
g	—	Redlich–Peterson isotherm exponent
ΔG	—	Gibbs energy
ΔH	—	Change in enthalpy
ΔS	—	Change in Entropy

References

[1] S.S. Muhamad, I. Suzylawati, Equilibrium, kinetic and thermodynamic studies of analgesic removal by thin coated activated carbon, J. Eng. Sci., 16 (2020) 47–63.
[2] S.K. Khetan, T.J. Collins, Human pharmaceuticals in the aquatic environment: a challenge to green chemistry, Chem. Rev., 107 (2007) 2319–2364.
[3] M. Carballa, F. Omil, J.M. Lema, M.A. Llompart, C. Garcıa-Jares, I. Rodrıguez, M. Gomez, T. Ternes, Behavior of pharmaceuticals, cosmetics and hormones in a sewage treatment plant, Water Res., 38 (2004) 2918–2926.
[4] J.L. Tambosi, L.Y. Yamanaka, H.J. José, R. de Fátima Peralta Muniz Moreira, H.F. Schröder, Recent research data on the removal of pharmaceuticals from sewage treatment plants (STP), Quím. Nova, 33 (2010) 411–420.
[5] F.O. Agunbiade, B. Moodley, Pharmaceuticals as emerging organic contaminants in umgeni river water system, KwaZulu-Natal, South Africa, Environ. Monit. Assess., 186 (2014) 7273–7291.
[6] B.P. Gumbi, B. Moodley, G. Birungi, P.G. Ndungu, Detection and quantification of acidic drug residues in South African surface water using gas chromatography-mass spectrometry, Chemosphere, 168 (2017) 1042–1050.
[7] V.P. Kasperchik, A.L. Yaskevich, A.V. Bildyukevich, Wastewater treatment for removal of dyes by coagulation and membrane processes, Pet. Chem., 52 (2012) 545–556.
[8] S. Nadupalli, N. Koorbanally, S.B. Jonnalagadda, Chlorine dioxide-facilitated oxidation of the azo dye amaranth, J. Phys. Chem. A, 115 (2011) 11682–11688.
[9] M. Imran, M.M. Iqbal, J. Iqbal, N.S. Shah, Z.U.H. Khan, B. Murtaza, M. Amjad, S. Ali, M. Rizwan, Synthesis, characterization and application of novel MnO and CuO impregnated biochar composites to sequester arsenic (As) from

water: modeling, thermodynamics and reusability, J. Hazard. Mater., 401 (2021) 123338, doi: 10.1016/j.jhazmat.2020.123338.
[10] Md. Ahmaruzzaman, Adsorption of phenolic compounds on low-cost adsorbents: a review, Adv. Colloid Interface Sci., 143 (2008) 48–67.
[11] A. Bhatnagar, A.K. Jain, A comparative adsorption study with different industrial wastes as adsorbents for the removal of cationic dyes from water, J. Colloid Interface Sci., 281 (2005) 49–55.
[12] A. Bhatnagar, M. Sillanpää, Utilization of agro-industrial and municipal waste materials as potential adsorbents for water treatment—a review, Chem. Eng. J., 157 (2010) 277–296.
[13] K.S. Smith, Chapter 7 – Metal Sorption on Mineral Surfaces: An Overview with Examples Relating to Mineral Deposits, Reviews in Economic Geology, Volumes 6A and 6B, The Environmental Geochemistry of Mineral Deposits Part A: Processes, Techniques, and Health Issues, Part B: Case Studies and Research Topics, Published by the Society of Economic Geologists, Inc. (SEG), 1999, pp. 161–182.
[14] J. Mittal, R. Ahmad, M.O. Ejaz, A Mariyam, A Mittal, A novel, eco-friendly bio-nanocomposite (Alg-Cst/Kal) for the adsorptive removal of crystal violet dye from its aqueous solutions, Int. J. Phytorem., 10 (2021), doi: 10.1080/15226514.2021.1977778.
[15] J. Mittal, A. Mittal, Batch and bulk adsorptive removal of anionic dye using metal/halide-free ordered mesoporous carbon as adsorbent, J. Cleaner Prod., 321 (2021) 129060, doi: 10.1016/j.jclepro.2021.129060.
[16] A. Mariyam, J. Mittal, F. Sakina, R.T. Baker, A.K. Sharma, Fixed-bed adsorption of the dye Chrysoidine R on ordered mesoporous carbon, Desalination, 229 (2021) 395–400.
[17] A. Mariyam, A Mittal, Efficient batch and fixed-bed sequestration of a basic dye using a novel variant of ordered mesoporous carbon as adsorbent, Arabian J. Chem., 14 (2021) 103186, doi: 10.1016/j.arabjc.2021.103186.
[18] A. Mariyam, J. Mittal, F. Sakina, R.T. Baker, A.K. Sharma, Adsorption behaviour of Chrysoidine R dye on a metal/halide-free variant of ordered mesoporous carbon, Desalination, 223 (2021) 425–433.
[19] I. Anastopoulos, I. Pashalidis, A.G. Orfanos, I.D. Manariotis, T. Tatarchuk, L. Sellaoui, A. Bonilla-Petriciolet, A. Mittal, A. Núñez-Delgado, Removal of caffeine, nicotine and amoxicillin from (waste)waters by various adsorbents. A review, J. Environ. Manage., 261 (2020) 110236, doi: 10.1016/j.jenvman.2020.110236.
[20] J. Mittal, Recent progress in the synthesis of layered double hydroxides and their application for the adsorptive removal of dyes: a review, J. Environ. Manage., 295 (2021) 113017, doi: 10.1016/j.jenvman.2021.113017.
[21] A. Mittal, R. Ahmad, I. Hasan, Iron oxide impregnated dextrin nanocomposite synthesis and its application for the biosorption of Cr(VI) ions from aqueous solution, Desalination, 57 (2016) 15133–15145.
[22] H. Boumediene, A Mittal, J. Mittal, A. Paolone, Synthesis and characterisation of egg shell (ES) and egg shell with membrane (ESM) modified by ionic liquids, Chem. Data Collect., 33 (2021) 100717, doi: 10.1016/j.cdc.2021.100717.
[23] V.K. Gupta, S. Agarwal, R. Ahmad, A. Mizzal, J. Mittal, Sequestration of toxic congo red dye from aqueous solution using eco-friendly guar gum/activated carbon nanocomposite, Int. J. Biol. Macromol., 8130 (2020) 33167, doi: 10.1016/j.ijbiomac.2020.05.025.
[24] P. Saharan, V. Kumar, J. Mittal, V. Sharma, A.K. Sharma, Efficient ultrasonic assisted adsorption of organic pollutants employing bimetallic carbon nanocomposites, Sep. Sci. Technol., 56 (2021) 2895–2908.
[25] S. Soni, P.K. Bajpai, J. Mittal, C. Arora, Utilisation of cobalt doped iron based MOF for enhanced removal and a recovery of methylene blue dye from waste water, J. Mol. Liq., 314 (2020) 113642, doi: 10.1016/j.molliq.2020.113642.
[26] H. Feather, A Remarkable Adsorbent for Dye Removal Chapter in Book: Green Chemistry for Dyes Removal from Wastewater, Dr. S.K. Sharma, Ed., Scrivener Publishing LLC, USA, 2015, pp. 409–457.
[27] G. Crini, P.M. Badot, Eds., Sorption Processes and Pollution, PUFC, Besançon, 2010, p. 489.
[28] G.Y. Kyzas, M. Kostoglou, Green adsorbents for wastewaters: a critical review, Materials, 7 (2014) 333–364.
[29] S.D. Khattri, M.K. Singh, Removal of malachite green from dye wastewater using neem sawdust by adsorption, J. Hazard. Mater., 167 (2009) 1089–1094.
[30] T.A Davis, B. Volesky, A. Mucci, A review of the biochemistry of heavy metal biosorption by brown algae, Water Res., 37 (2003) 4311–4330.
[31] M. Grassi, G. Kaykioglu, V. Belgiorno, G. Lofrano, Removal of Emerging Contaminants from Water and Wastewater by Adsorption Process, G. Lofrano, Ed., Emerging Compounds Removal from Wastewater, Springer Briefs in Molecular Science, Springer, Dordrecht, 2012.
[32] K. Chojnacka, Biosorption of Cr(III) ions by eggshells, J. Hazard. Mater. B, 121 (2005) 167–173.
[33] A.G.J. Tacon, Utilisation of chick hatchery waste: the nutritional characteristics of day-old chicks and egg shells, Agric. Wastes, 4 (1982) 335–343.
[34] R.B. Christmas, R.H. Harms, Utilization of egg shells and phosphoric acids as a source of phosphorus and calcium in the diet of White Leghorn cockerels, Poult. Sci., 55 (1976) 264–267.
[35] H.A. Hegazi, Removal of heavy metals from wastewater using agricultural and industrial wastes as adsorbents, HBRC J., 9 (2013) 276–282.
[36] V. Vimonses, S. Lei, B. Jin, C.W.K. Chow, C. Saint, Kinetic study and equilibrium isotherm analysis of Congo Red adsorption by clay materials, Chem. Eng. J., 148 (2009) 354–364.
[37] C.H. Zhou, J. Keeling, Fundamental and applied research on clay minerals: from climate and environment to nanotechnology, Appl. Clay Sci., 74 (2013) 3–9.
[38] M.N. Chong, B. Jin, C.W.K. Chow, C. Saint, Recent developments in photocatalytic water treatment technology: a review, Water Res., 44 (2010) 2997–3027.
[39] I. Zhu, T. Getting, A review of nitrate reduction using inorganic materials, Environ. Technol. Rev., 1 (2012) 46–58.
[40] R. Bhaumik, N.K. Mondal, B. Das, P.G. Roy, K.C. Pal, C. Das, A. Banerjee, J.K. Datta, Eggshell powder as an adsorbent for removal of fluoride from aqueous solution: equilibrium, kinetic and thermodynamic studies, E-J. Chem., 9 (2012) 790401, doi: 10.1155/2012/790401.
[41] A.V. Borhade, A.S. Kale, Calcined eggshell as a cost effective material for removal of dyes from aqueous solution, Appl. Water Sci., 7 (2012) 4255–4268.
[42] B.Z. Butt, Nanotechnology and Waste Water Treatment, S. Javad, Ed., Nanoagronomy, Springer, Cham, 2020.
[43] C. Trois, A. Cibati, South African sands as an alternative to zero valent iron for arsenic removal from an industrial effluent: batch experiments, J. Environ. Chem. Eng., 3 (2015) 488–498.
[44] O.A. Oyetade, V.O. Nyamori, B.S. Martincigh, S.B. Jonnalagadda, Effectiveness of carbon nanotube–cobalt ferrite nanocomposites for the adsorption of rhodamine B from aqueous solutions, RSC Adv., 5 (2015) 22724–22739.
[45] Y.S. Ho, Removal of copper ions from aqueous solution by tree fern, Water Res., 37 (2003) 2323–2330.
[46] J. Lin, L. Wang, Comparison between linear and non-linear forms of pseudo-first-order and pseudo-second-order adsorption kinetic models for the removal of methylene blue by activated carbon, Front. Environ. Sci. Eng., 3 (2009) 320–324.
[47] A. Dabrowski, Adsorption—from theory to practice, Adv. Colloid Interface Sci., 93 (2001) 135–224.
[48] K.H. Boparai, M. Joseph, D.M. O'Carroll, Kinetics and thermodynamics of cadmium ion removal by adsorption onto nanozerovalent iron particles, J. Hazard. Mater., 186 (2010) 458–465.
[49] K. Vijayaraghavan, R. Balasubramanian, Is biosorption suitable for decontamination of metal-bearing wastewaters? A critical review on the state-of-the-art of biosorption processes and future directions, J. Environ. Manage., 160 (2015) 283–296.
[50] N. Ayawei, A.T. Ekubo, D. Wankasi, E.D. Dikio, Adsorption of Congo red by Ni/Al-CO_3: equilibrium, thermodynamic and kinetic studies, Orient. J. Chem., 31 (2015) 1307–1318.

[51] T.M. Elmorsi, Equilibrium isotherms and kinetic studies of removal of methylene blue dye by adsorption onto miswak leaves as a natural adsorbent, J. Environ. Prot., 2 (2011) 817–827.
[52] V. Kuppusamy, T. Padmesh, K. Palanivelu, K.V. Manickam, Biosorption of nickel(II) ions onto *Sargassum wightii*: application of two-parameter and three-parameter isotherm models, J. Hazard. Mater., 133 (2006) 304–308.
[53] A. Botea-Petcu, S. Tanasescu, V. Varazashvili, N. Lejava, T. Machaladze, M. Khundadze, F. Maxim, F. Teodorescu, J. Martynczuk, Z. Yáng, L.J. Gauckler, Thermodynamic data of $Ba_{0.6}Sr_{0.4}Co_{0.8}Fe_{0.2}O_{3-\delta}$ SOFC cathode material, Mater. Res. Bull., 57 (2014) 184–189.
[54] L. Shuyan, L. Zhe, H. Xiqiang, W. Bo, S. Wenhui, Electrical and thermal properties of $(Ba_{0.5}Sr_{0.5})_{1-x}Sm_xCo_{0.8}Fe_{0.2}O_{3-\delta}$ perovskite oxides, Solid State Ionics, 178 (2007) 417–422.
[55] S. Zongping, X. Guoxing, T. Jianghua, D. Hui, Y. Weishen, Ba effect in doped $Sr(Co_{0.8}Fe_{0.2})O_{3-\delta}$ on the phase structure and oxygen permeation properties of the dense ceramic membranes, Sep. Purif. Technol., 25 (2001) 419–429.
[56] S. Trasatti, Electrocatalysis by oxides – attempt at a unifying approach, J. Electroanal. Chem., 1119 (1980) 125–131.
[57] W. Zhou, M. Zhao, F. Liang, S.C. Smith, Z. Zhu, High activity and durability of novel perovskite electrocatalysts for water oxidation, Mater. Horiz., 2 (2015) 495–501.
[58] H.D. Lutz, H. Möller, M. Schmidt, Lattice vibration spectra. Part LXXXII. Brucite-type hydroxides $M(OH)_2$ (M = Ca, Mn, Co, Fe, Cd) — IR and Raman spectra, neutron diffraction of $Fe(OH)_2$, J. Mol. Struct., 328 (1994) 121–132.
[59] M.K. Johnson, D.B. Powell, R.D. Cannon, Vibrational spectra of carboxylate complexes—III. Trinuclear 'basic' acetates and formates of chromium(III), iron(III), and other transition metals, Spectrochim. Acta, Part A, 37 (1981) 995–1006.
[60] I.A.A. Hamza, B.S. Martincigh, J.C. Ngila, V.O. Nyamori, Adsorption studies of aqueous Pb(II) onto a sugarcane bagasse/multi-walled carbon nanotube composite, Phys. Chem. Earth, 66 (2013) 157–166.
[61] Y.S. Ho, G. McKay, Kinetic models for the sorption of dye from aqueous solution by wood process, Process Saf. Environ. Prot., 76 (1998) 183–191.
[62] E. Demirbas, M. Kobya, E. Senturk, T. Ozkan, Adsorption kinetics for the removal of chromium(VI) from aqueous solutions on the activated carbons prepared from agricultural wastes, Water SA, 30 (2004) 533–539.
[63] S.H. Chien, W.R. Clayton, Application of Elovich equation to the kinetics of phosphate release and sorption in soils, Soil Sci. Soc. Am. J., 44 (1980) 265–268.
[64] R. Krishna, A unified approach to the modelling of intraparticle diffusion in adsorption processes, Gas Sep. Purif., 7 (1993) 91–104.
[65] Y. Yao, F. Xu, M. Chen, Z. Xu, Z. Zhu, Adsorption behaviour of methylene blue on carbon nanotubes, Bioresour. Technol., 101 (2010) 3040–3046.
[66] C.H. Wu, Adsorption of reactive dye onto carbon nanotubes: equilibrium, kinetics and thermodynamics, J. Hazard. Mater., 144 (2007) 93–100.
[67] S.G. Muntean, M.E. Radulescu-Grad, P. Sfarloaga, Dye adsorbed on copolymer, possible specific sorbent for metal ions removal, RSC Adv., 4 (2014) 27354–27362.
[68] K.S. Moaaz, B. Mariusz, A. Ioannis, A.G. Dimitrios, A novel nanocomposite of activated serpentine mineral decorated with magnetic nanoparticles for rapid and effective adsorption of hazardous cationic dyes: kinetics and equilibrium studies, Nanomaterials, 10 (2020) 684, doi: 10.3390/nano10040684.
[69] Z. Zhao, Z. Yang, Y. Hu, J. Li, X. Fan, Multiple functionalization of multi-walled carbon nanotubes with carboxyl and amino groups, Appl. Surf. Sci., 276 (2013) 476–481.
[70] Y. Zhang, H. He, C. Gao, J. Wu, Covalent layer-by-layer functionalization of multiwalled carbon nanotubes by click chemistry, Langmuir, 25 (2009) 5814–5824.
[71] H.M.F. Freundlich, Over the adsorption in solution, Z. Phys. Chem., 57 (1906) 385–470.
[72] I. Langmuir, The adsorption of gases on plane surfaces of glass, mica and platinum, J. Am. Chem. Soc., 409 (1918) 1361–1402.
[73] M.I. Templin, V. Pyzhev, Kinetics of ammonia synthesis on promoted iron catalyst, Acta Phys. Chim. USSR, 12 (1940) 327–356.
[74] M.M. Dubinin, The potential theory of adsorption of gases and vapors for adsorbents with energetically non uniform surface, Chem. Rev., 60 (1960) 235–266.
[75] J. Toth, State equation of the solid gas interface layer, Acta Chim. Hungaricae, 69 (1971) 311–317.
[76] M. Davoundinejad, S.A. Gharbanian, Modelling of adsorption isotherm of benzoic compounds onto GAC and introducing three new isotherm models using new concepts of adsorption effective surface (AEC), Acad. J., 46 (2013) 2263–2275.
[77] M. Dutta, U. Das, S. Mondal, Adsorption of acetaminophen by using tea waste derived activated carbon, Int. J. Environ. Sci., 2 (2015) 270–281.
[78] D.T. Nguyen, H. Nguyen Tran, R.-S. Juang, N. Duy Dat, F. Tomul, A. Ivanets, S. Han Woo, A. Hosseini-Bandegharaei, V. Phuong Nguyen, H.-P. Chao, Adsorption process and mechanism of acetaminophen onto commercial activated carbon, J. Environ. Chem. Eng., 6 (2020) 104408, doi: 10.1016/j.jece.2020.104408.
[79] H.B. Quesada, L.F. Cusioli, C. de O. Bezerra, A.T.A. Baptista, L. Nishi, R.G. Comes, R. Bergamasco, Acetaminophen adsorption using a low cost adsorbent prepared from modified residues of *Moringa oleifera* Lam. seed husks, J. Chem. Technol. Biotechnol., 10 (2010) 3147–3157.
[80] C.A. Rey-Mafull, J.E. Tacoronte, R. Garcia, J. Tobella, J.C. Llópiz, A. Iglesias, D. Hotza, Comparative study of the adsorption of acetaminophen on activated carbons in simulated gastric fluid, SpringerPlus, 48 (2014) 1–12.
[81] D.M. Juela, Comparison of the adsorption capacity of acetaminophen on sugarcane bagasse and corn cob by dynamic simulation, Sustainable Environ. Res., 30 (2020) 23, doi: 10.1186/s42834-020-00063-7.
[82] A. Parus, M. Gaj, B. Karbowska, J. Zembrzuska, Investigation of acetaminophen adsorption with a biosorbent as a purification method of aqueous solution, Chem. Ecol., 7 (2020) 705–725.
[83] S.O. Akpotu, B. Moodley, Application of as-synthesized MCM-41and MCM-41 wrapped with reduced graphene oxide/graphene oxide in the remediation of acetaminophen and aspirin from aqueous system, J. Environ. Manage., 209 (2018) 205–215.
[84] P.W. Atkins, Essentials of Physical Chemistry, 4th ed., Oxford University Press, Oxford, 2001.
[85] S. Annamária, H. Éva, C. Martina, F. Attila, The correctness of Van't Hoff plots in chiral and achiral chromatography, J. Chromatogr., A, 1611 (2020) 460594, doi: 10.1016/j.chroma.2019.460594.
[86] Y. Liu, Y.J. Liu, Biosorption isotherms, kinetics and thermodynamics, Sep. Purif. Technol., 61 (2008) 229–242.

Supplementary information

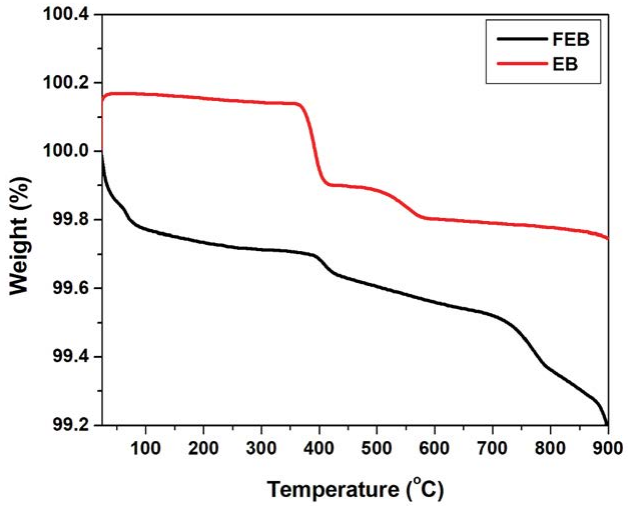

Fig. S1. The thermogravimetric (TGA) analysis of FEB and EB nanocomposite calcined at 1,000°C for 5 h.

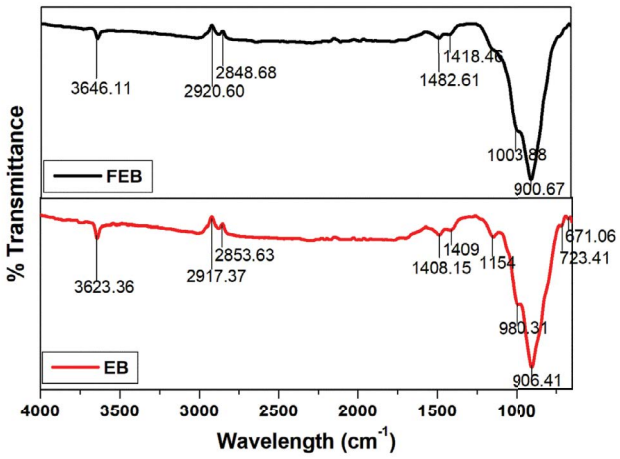

Fig. S2. The FTIR analysis of FEB and EB nanocomposite calcined at 1,000°C for 5 h.

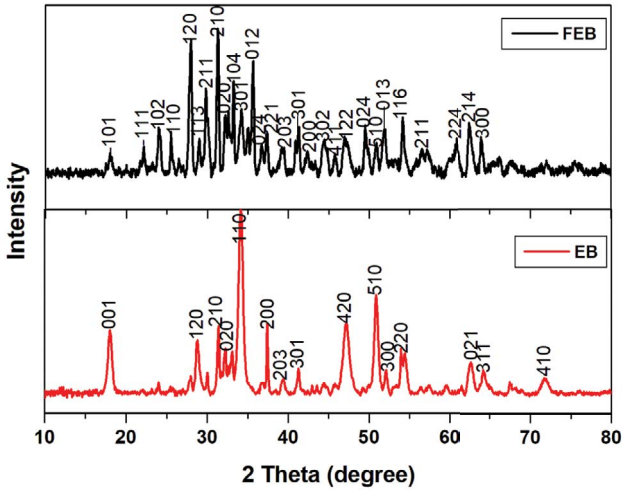

Fig. S3. The X-ray diffraction (XRD) analysis of (a) FEB and (b) EB nanocomposites calcined at 1,000°C for 5 h.